ISSN: 2993-8643

Research Article

Engineering: Open Access

Numerical Investigation of Fin Shape Optimization and Entropy of Magnetohydrodynamics Natural Convection Nanofluid Flow in a Cavity

Bai Mbye Cham[1,4*], Shafee Ahmad[2], Shams-ul-Islam[1], Afraz Hussain Majeed[2], M. Saleem[3], Dawda Charreh[1,4] and Sainabou Ngack[4]

[1]*Department of Mathematics, COMSATS University Islamabad, Park Road, Tarlai Kalan, Islamabad 44000, Pakistan.*

[2]*School of Energy and Power Engineering, Jiangsu University, Zhenjiang 212013, China*

[3]*Department of Science and Humanities, Sir Syed CASE Institute of Technology, Pakistan.*

[4]*Department of Mathematics, University of The Gambia, P.O. Box 3530, Serrekunda, The Gambia.*

[*]Corresponding Author
Bai Mbye Cham, Department of Mathematics, COMSATS University Islamabad, Park Road, Tarlai Kalan, Islamabad, Pakistan

Submitted: 2023, Oct 20; **Accepted**: 2023, Nov 27; **Published**: 2023, Dec 05

Citation: Cham, B. M., Ahmad, S., Saleem, M., Majeed, A. H., Charreh, D. et al. (2023). Numerical Investigation of Fin Shape Optimization and Entropy of Magnetohydrodynamics Natural Convection Nanofluid Flow in a Cavity. *Eng OA, 1*(4), 203-220.

Abstract

The purpose of the investigation is to analyze the effect of fin length and position in terms of rotational angle on heat transmission and entropy generation. Different parameters such as Prandtl numbers, Hartmann numbers, Rayleigh numbers, and particle volume fractions are used to analyze nanofluid laminar flow behavior and temperature distribution. The fin has a significant impact on both the isotherm and the streamlines. Findings revealed that increasing the rotational angle of a spinning heat exchanger might result in more consistent temperature distribution along isotherms; larger fins, on the other hand, frequently provide greater heat dissipation due to increased surface area. Furthermore, when Rayleigh numbers increase, so does the temperature distribution between the fins and the surrounding fluid. The presence of a magnetic field affects fluid dynamics and contributes to the generation of entropy. Higher Prandtl numbers can result in the enhancement heat transfer phenomena and the generation of entropy.

Keywords: Cavity; Entropy; Fins; Magnetohydrodynamics; Natural Convection Nanofluid.

1. Introduction

Fins are characterized as expanded surfaces affixed to the enclosure's walls to improve heat transmission. They improve the available surface area for heat exchange between the fluid and its surroundings. The researchers have recently focused on the influence of fin attachment angle, thickness, and depth of fins on heat transfer processes [1, 2]. Tayebs et al. investigated the effects of magnetic fields and fin geometry on the thermo-economic performance and entropy generation of natural convective flow in a nanofluid-filled circular enclosure [3]. Ye et al. investigated arrow-shaped fins that affect the melting performance of thermal heat energy storage units. For improved heat transmission, a heat exchanger with wavy-shaped fins and elliptical tubes was used and the results obtained prove that fins and elliptic tubes could significantly affect heat transmission [4-6].

Flows in general are affected by the movement of their particles. These effects might be noticed generally in fluid square cavity situations with many interior obstacles. This necessitates the use of a proper numerical method that accounts for the size, mobility, location, and position of items on flows. Dimensionless parameters are useful tools for analyzing fluid flow issues. Muhammad et al. studied dimensionless quantities and a homotopic optimal procedure was applied to his mathematical model [7]. The results presented showed a general increase in skin friction and Nusselt number. Ganesh et al. conducted a numerical incompressible flow of water on viscous ohmic dissipation in a boundary layer approximation [8]. The studies reveal that suction parameters and

local inertia coefficient provide unique solutions. The effect of skin friction, Nusselt number, and temperature was found to be in conformity with the benchmark. Hossain et al. investigated the effect of drag ratio which has a significant impact only if there exists a reduction in the flow composition [9]. Abu-Nada et al. confirmed that the average Nusselt number has a greater impact on viscosity than the thermal conductivity model. Khanafer et. al. discuss a group of different parameters which were used to investigate the general heat transfer effect on a two-dimensional (2D) enclosure [11].

The study of the interaction of magnetic fields with electrically conductive fluids is known as Magnetohydrodynamics (MHD). Bio-medical applications and detective systems of magnetic effects have recently attracted interest in the field of fluid mechanics. Kuwahata et al. observed a sensitive cavity shape magnetic sensor characterized for detection ability. A numerical simulation was conducted and exposed a wide range of magnetic null points on the cavity problems [12]. The authors reveals that a strong gradient of magnetic field reduces to approximately zero for cavity shape magnets. The problems suggest the application of strong magnetic sensors for accurate detection in all fields of biomedical application. Geridonmez et al. demonstrate spontaneous convection in a porosity-filled square cavity under a partial magnetic field [13]. Heat transfer rate is usually influenced by magnetic field radiation and joules heating. Dutta et al. investigated the numerical simulation of magnetohydrodynamic buoyancy induce convection in a quadrantal hallow filled with a nanofluid [14]. MHD natural convection on enclosures has arouse the curiosity of many scientists in recent decades since it occurs in a variety of technological applications such as the nuclear reactors and liquid metal cooling [15-21].

Entropy which is generally classified as an irreversible process has recently attracted interest from researchers in the field of fluid flows. Baytas observed that local entropy generation was a significant determinant for the angle of inclination [22]. Baytas also studied the reduction of entropy generation for different situations using thermodynamics. Shah et al. investigated a conducting electrical nano-fluids with entropy optimization events [23, 24]. The authors reveal the inverse relationship between the given Bejan number and permeability, the impact of Brownian motion on nano-fluids, and a strong application of entropy in engineering and technology. Saleem et al. and Alzahrani et al. studied entropy generation and significant results were obtained [25, 26]. The authors concluded that the temperature gradient is the main determinant of entropy generation.

Natural convection significantly impacts the temperature ratio contribution to the resistance of inertia on surface radiation. Natural convection for thermo-capillary force and Newtonian flow on a cavity problem was an area of concern. The effect of buoyancy which is characterized by a rise and fall in an enclosed path was crucial in the movement of the fluid. Stampolidis et al. show a significant difference between dynamic viscosity enhancement and thermal conductivity was found to be useful [27]. The authors discussed the error, stability, and consistency of different methods in line with the results obtained. Ho et al. examines the effect of shear stress and strains and thermal conductivity of fluids on natural convection [28]. Mahmoodi et al. investigated free convection on heat transfer processes in a square hallow filled with a nanofluid. The inclusion of the adiabatic square block in the cavity alters the temperature gradients and flow patterns [29].

The primary objective of this research is to look at the impact of fin length and position in terms of rotational angle on heat transmission and entropy generation using nanofluids. Different dimensionless parameters will be used to analyze flow behavior and temperature distribution. The mathematical formulation, entropy generation, code validation, results and discussion will be the thematic areas of our research studies. Incorporating the magnetic effect as well as analysis the entropy generation effects on nanofluids where key to our numerical simulation and results interpretation.

2. Mathematical Formulation

2.1 Statement of Problem

The flow is considered two-dimensional, steady state, uniform, incompressible and laminar. The problem of natural convection and entropy generation in a 2D square cavity of length (L = 1) is considered. The cavity has a circular shaped tube at the center with a fixed radius r = 0.1. Four similar fins of length l/2 and width w lie at the center of the cavity placed perpendicular to each other. The width of the fin is taken as w = 0.02 while its length lies in the range between $0.2 \leq l \leq 0.5$. The rotational angle is varied between $0^0 \leq \alpha \leq 90^0$. Figure 1 is a schematic representation of the problem statement. The magnetic field with a strength B0 was applied on the left vertical wall towards the horizontal direction. The right wall is under the influence of constant higher temperature (T_h) and the left wall is under the influence of constant cooled temperature (T_c). The top and bottom of the enclosure are assumed adiabatic.

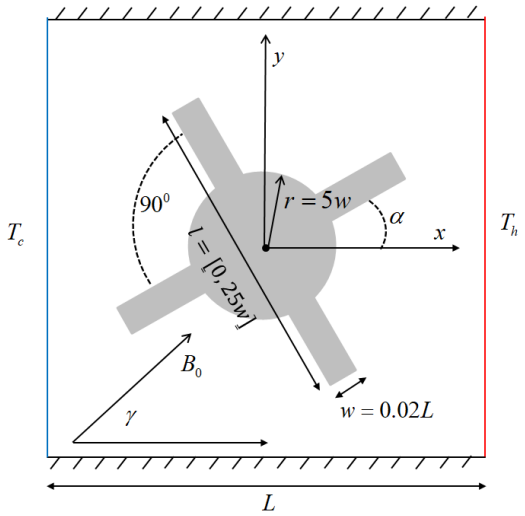

Figure 1: Schematic representation of the proposed problem

2.2. Governing equations in dimensional form

The governing equations for dimensionless forms in nanofluids generally contain mass, momentum, and energy conservation equations, which are stated in dimensionless form using suitable scaling factors. These dimensionless equations are then numerically solved using appropriate numerical methods to get solutions for velocity, pressure, temperature, and other variables in the nanofluid flow. Equation (1) to (4) represents the governing equations for the nanofluid problem [11, 14, 32, 33].

$$\frac{\partial u}{\partial x}+\frac{\partial v}{\partial y}=0 \tag{1}$$

$$\frac{\partial u}{\partial t}+u\frac{\partial u}{\partial x}+v\frac{\partial u}{\partial y}=-\frac{1}{\rho}\frac{\partial p}{\partial x}+\frac{\mu_{mix}}{\rho_{mix}}\left(\frac{\partial^2 u}{\partial x^2}+\frac{\partial^2 u}{\partial y^2}\right) \tag{2}$$

$$\frac{\partial v}{\partial t}+u\frac{\partial v}{\partial x}+v\frac{\partial v}{\partial y}=-\frac{1}{\rho}\frac{\partial p}{\partial y}+\frac{\mu_{mix}}{\rho_{mix}}\left(\frac{\partial^2 v}{\partial x^2}+\frac{\partial^2 v}{\partial y^2}\right)-\frac{\sigma_{mix}B_0^2}{\rho_{mix}}v+\frac{(\rho\beta)_{mix}}{\rho_{mix}}g(T-T_0) \tag{3}$$

$$\frac{\partial T}{\partial t}+u\frac{\partial T}{\partial x}+v\frac{\partial T}{\partial y}=\frac{k_{mix}}{(\rho C_p)_{mix}}\left(\frac{\partial^2 T}{\partial x^2}+\frac{\partial^2 T}{\partial y^2}\right) \tag{4}$$

where u and v are the velocity components of the nanofluid along the dimensional x and y directions. Other dimensional values include fluid pressure (p) and temperature (T). The non-Newtonian nanofluid's density, effective dynamic viscosity, permeability, thermal expansion coefficient, temperature, and specific heat are represented by the value ρ_{mix}, μ_{mix} , k_{mix}, β, T, and C_p, respectively. β_0 and σ_{mix} is the constant attached to the magnet effect.

The purpose of the nanofluid model is to represent the increased thermal and flow characteristics of nanoscale suspensions, which makes them appealing for a variety of engineering applications. The model accounts for the interactions between the base fluid and the nanoparticles, including the impacts on heat transfer, fluid flow, and other important phenomena. Equation (5) to (10) shows the nanofluid equations for our problem [14, 33].

$$\rho_{mix}=(1-\phi)\rho_f+\phi\rho_s \tag{5}$$

$$(\rho C_p)_{mix}=(1-\varphi)(\rho C_p)_f+\phi(\rho C_p)_s \tag{6}$$

$$(\rho\beta)_{mix}=(1-\varphi)(\rho\beta)_f+\phi(\rho\beta)_s \tag{7}$$

$$\sigma_{mix}=(1-\phi)\sigma_f+\phi\sigma_s \tag{8}$$

$$\mu_{mix} = \frac{\mu_f}{(1-\phi)^{2.5}} \tag{9}$$

$$\frac{k_{mix}}{k_f} = \frac{k_s + 2k_f - 2\phi(k_f - k_s)}{k_s + 2k_f + \phi(k_f - k_s)} \tag{10}$$

where ϕ represents the nanoparticle volume fraction in the base fluid, and the subscripts *f*, *mix*, and *s* reflect the parameters of the base fluid, nanofluid, and nanoparticles, respectively.

2.3 Dimensionless Variables

In non-dimensional expression, the controlling equation are change to dimensionless form by the dimensionless parameters. The following non-dimensional variables are considered for the problem [11]:

$$\bar{x} = \frac{x}{L}\ ,\ \bar{y} = \frac{y}{L}\ ,\ \bar{u} = \frac{uL}{\alpha}\ ,\ \bar{v} = \frac{vL}{\alpha}\ ,\ \bar{p} = \frac{pL^2}{\rho\alpha^2}\ ,\ \theta = \frac{T - T_0}{T_h - T_0}\ ,\ \nu = \frac{\mu}{\rho},\ \alpha = \frac{k}{\left(\rho C_p\right)},\ Pr = \frac{\nu}{\alpha}$$

$$Ra = \frac{g\beta_f L^3\left(T_h - T_c\right)}{\nu_f \alpha_f},\ Ha^2 = B_0 L\sqrt{\frac{\sigma_{mix}}{\rho_{mix}\nu_f}}, \tag{11}$$

Using the above dimensionless parameters defined in Eq. (11) and applying them to the governing Eq. (1) to (4) we obtained Eq. (12) to (15)

$$\frac{\partial \bar{u}}{\partial \bar{x}} + \frac{\partial \bar{v}}{\partial \bar{y}} = 0 \tag{12}$$

$$\frac{\partial \bar{u}}{\partial \bar{t}} + \bar{u}\frac{\partial \bar{u}}{\partial \bar{x}} + \bar{v}\frac{\partial \bar{u}}{\partial \bar{y}} = -\frac{\partial \bar{p}}{\partial \bar{x}} + \frac{\left(\frac{\mu}{\rho}\right)_{mix}}{\left(\frac{\mu}{\rho}\right)_f} Pr\left(\frac{\partial^2 \bar{u}}{\partial \bar{x}^2} + \frac{\partial^2 \bar{u}}{\partial \bar{y}^2}\right) \tag{13}$$

$$\frac{\partial \bar{v}}{\partial \bar{t}} + \bar{u}\frac{\partial \bar{v}}{\partial \bar{x}} + \bar{v}\frac{\partial \bar{v}}{\partial \bar{y}} = -\frac{\partial \bar{p}}{\partial \bar{x}} + \frac{\left(\frac{\mu}{\rho}\right)_{mix}}{\left(\frac{\mu}{\rho}\right)_f} Pr\left(\frac{\partial^2 \bar{v}}{\partial \bar{x}^2} + \frac{\partial^2 \bar{v}}{\partial \bar{y}^2}\right) - Ha^2 Pr\bar{v} + \left(1 - \emptyset + \emptyset\left(\frac{(\rho\beta)_{mix}}{(\rho\beta)_f}\right)\right)\theta \tag{14}$$

$$\frac{\partial \theta}{\partial \bar{t}} + \bar{u}\frac{\partial \theta}{\partial \bar{x}} + \bar{v}\frac{\partial \theta}{\partial \bar{y}} = \frac{\left(\frac{k}{\rho c_p}\right)_{mix}}{\left(\frac{k}{\rho c_p}\right)_f}\left(\frac{\partial^2 \theta}{\partial \bar{x}^2} + \frac{\partial^2 \theta}{\partial \bar{y}^2}\right) \tag{15}$$

where $\bar{u}$ and $\bar{v}$ represent the flow's non-dimensional velocities as well as the non-dimensional $\bar{x}$ and $\bar{y}$ directions.

The nanoparticle is represented as $\emptyset$. The values of $\left(\frac{\mu}{\rho}\right)_{mix}$ and $\nu_f = \left(\frac{\mu}{\rho}\right)_f$ reflect the nanofluid and base fluid's kinematic viscosities respectively. while $\left(\frac{k}{\rho c_p}\right)_{mix}$ *and* $\left(\frac{k}{\rho c_p}\right)_f$ represent thermal diffusivity for nanofluid and base fluid respectively. The dimensionless temperature and pressure are indicated by θ and $\bar{p}$. The non-dimensional parameters *Pr*, *Ra*, and *Ha* represent the base fluid's Prandtl number, Rayleigh number of thermal expansion, and Hartmann number, respectively.

3. Entropy Generation in Dimensional Form

The development of entropy during the flow of a nanofluid, which is a combination of a base fluid (typically a liquid) and nanoparticles with nanoscale dimensions, is referred to as entropy generation in nanofluids. The presence of nanoparticles in a fluid can alter its thermodynamic and transport characteristics, resulting in changes in entropy generation. Several parameters can impact entropy formation in nanofluids, including nanoparticle concentration, particle size, fluid flow velocity, and temperature gradient. The inclusion of nanoparticles can modify heat transmission and fluid flow behavior influencing entropy formation. Entropy generation will be obtained from entropy due to heat, fluid friction and magnetic effect. Equation (16) to (18) defines entropy generation for heat, fluid friction and magnet respectively [33]. Similarly, Table 1 shows the physical properties for fluids and nanoparticles of water and copper.

$$S_h = \frac{k_{mix}}{T_0^2}\left(\left(\frac{\partial T}{\partial x}\right)^2 + \left(\frac{\partial T}{\partial y}\right)^2\right) \tag{16}$$

Table 1: Physical properties of fluid and nanoparticles.

Property	Water	Copper
k (W/(m K))	0.613	401
ρ (kg/m^3)	997.1	8954
β (K^{-1})	2.1×10^{-4}	1.67×10^{-5}
C_p (J/(kg K))	4179	383
μ (kg/(ms))	8.91×10^{-5}	–
$\boldsymbol{\alpha}$ (m^2/s)	1.5×10^{-7}	1.1×10^{-4}

$$S_f = \frac{\mu_{mix}}{T_0}\left[2\left(\left(\frac{\partial u}{\partial x}\right)^2 + \left(\frac{\partial v}{\partial y}\right)^2\right) + \left(\frac{\partial u}{\partial y} + \frac{\partial v}{\partial x}\right)^2\right] \tag{17}$$

$$S_m = \frac{\sigma_{mix} B_0^2}{T_0} v^2 \tag{18}$$

Applying dimensionless forms defined in Eq. (11) to Eq. (16) to (18), then we obtained the dimensionless form for entropy due to heat, friction and magnet as presented in Eq. (19) to (21),

$$\bar{S}_h = \frac{k_{mix}}{k_f}\left(\left(\frac{\partial \theta}{\partial \bar{x}}\right)^2 + \left(\frac{\partial \theta}{\partial \bar{y}}\right)^2\right) \tag{19}$$

$$\bar{S}_f = \eta\left(\frac{\left(\frac{\mu}{\rho}\right)_{mix}}{\left(\frac{\mu}{\rho}\right)_f}\right)\left[2\left(\frac{\partial \bar{u}}{\partial \bar{x}}\right)^2 + 2\left(\frac{\partial \bar{v}}{\partial \bar{y}}\right)^2 + \left(\frac{\partial \bar{u}}{\partial \bar{y}} + \frac{\partial \bar{v}}{\partial \bar{x}}\right)^2\right] \tag{20}$$

$$\bar{S}_m = \eta Ha^2\left(\frac{\sigma_{mix}}{\sigma_f}\right)\bar{v} \tag{21}$$

Since total entropy is $\bar{S}_T = \bar{S}_h + \bar{S}_f + \bar{S}_m$ then we have Eq. (22) as

$$\bar{S}_T = \frac{k_{mix}}{k_f}\left(\left(\frac{\partial \theta}{\partial \bar{x}}\right)^2 + \left(\frac{\partial \theta}{\partial \bar{y}}\right)^2\right) + \eta\left(\frac{\left(\frac{\mu}{\rho}\right)_{mix}}{\left(\frac{\mu}{\rho}\right)_f}\right)\left[2\left(\frac{\partial \bar{u}}{\partial \bar{x}}\right)^2 + 2\left(\frac{\partial \bar{v}}{\partial \bar{y}}\right)^2 + \left(\frac{\partial \bar{u}}{\partial \bar{y}} + \frac{\partial \bar{v}}{\partial \bar{x}}\right)^2\right] + \eta Ha^2\left(\frac{\sigma_{mix}}{\sigma_f}\right)\bar{v}, \tag{22}$$

Equation (23) is the Bejan number ($\bar{S}_B$) is a dimensionless quantity in thermodynamics and heat transfer that quantifies the relative significance of convective ($\bar{S}_h$) and conductive ($\bar{S}_t$) heat transfer in a system. It is frequently related to the creation of entropy.

$$\bar{S}_B = \frac{\bar{S}_h}{\bar{S}_T} \tag{23}$$

The Brinkman number expresses the relevance of viscous dissipation in conductive heat transmission inside a porous material. A high Brinkman number indicates that viscous dissipation is more important than conductive heat transmission, whereas a low Brinkman number indicates that conductive heat transfer is more important and hence enhances entropy generation. Equation (24) is the Brinkman number and considered $\eta = 10^{-4}$

$$\eta = \frac{\mu_f T_0}{k_f}\left(\frac{k}{L(T_h - T_c)\rho c_p}\right)^2 \tag{24}$$

The initial and boundary conditions are given as in Khanafer et al [11] and Charreh et al. [31].
Initial values

$$u = v = \theta = 0 \text{ for } t = 0,$$

Boundary to the left wall.

$$x = 0,\ \psi = 0,\ \theta = 0,\ \omega = -\frac{\partial^2 \psi}{\partial x^2},$$

Boundary to the right wall

$$x = 1,\ \psi = 0,\ \theta = 1,\ \omega = -\frac{\partial^2 \psi}{\partial x^2},$$

Boundary at top and bottom walls

$$\psi = 0,\ \omega = -\frac{\partial^2 \psi}{\partial y^2},\ \frac{\partial \theta}{\partial y} = 0. \tag{25}$$

4. Solution Methodology and Grid Independence Study

In this research paper, the numerical method explored is the finite element method (FEM) applied to the nanofluid cavity problem with obstacles. The FEM involves discretizing the complex domain into smaller elements, such as quadrilaterals, and approximating the solution using interpolation functions known Abbas et al. [30]. The governing partial differential equations (PDEs) for fluid dynamics and heat transfer are transformed into their weak form and integrated over each element to create a global system of algebraic equations. Boundary conditions are imposed to obtain a unique solution. By incorporating nanofluid properties and obstacle modeling, the method allows for the analysis of flow behavior and heat transfer characteristics within the cavity. The numerical results provide insights into the behavior of nanofluids in the presence of obstacles and contribute to a deeper understanding of this complex problem. The grid study was made on local Nusselt number on the left cavity wall at $Pr = 6.2$, $Ra = 10^6$, $\phi = 0.02$, $Ha = 25$, and $\eta = 10^{-4}$ as in Fig 2. The first has merely a circular cylinder in the center, whereas the second has fins of length l/2 connected to the cylinder, as illustrated in fig. 3. For each number of grid elements chosen, the local and average Nusselt number was computed. Table 2 shows an insignificant change at both level 4 and 5. Hence the need for adopting level 4 for the remaining computation. The grid independence analysis assures that the computational results obtained from our results are resilient and not greatly impacted by grid spacing, hence improving the study's dependability and correctness. It ensures that the heat transfer increases seen are real, not artifacts of the numerical discretization procedure.

Table 2: Average Nusselt number on the left cavity wall with and without fin at $Pr = 6.2$, $Ra = 10^6$, $\phi = 0.02$, $Ha = 25$, and $\eta = 10^{-4}$

	No fin ($l = 0$)			with fin ($l = 0.5$)		
S.no	No. E	Dof	Nu_{avg}	No. E	Dof	Nu_{avg}
1	1020	2224	6.9996	1358	2980	7.0788
2	2240	4776	8.0445	2356	5088	8.0855
3	4336	9048	8.1495	4338	9148	8.1906
4	8390	17452	8.2633	8230	17260	8.3066
5	14048	28904	8.2605	13560	28088	8.3038

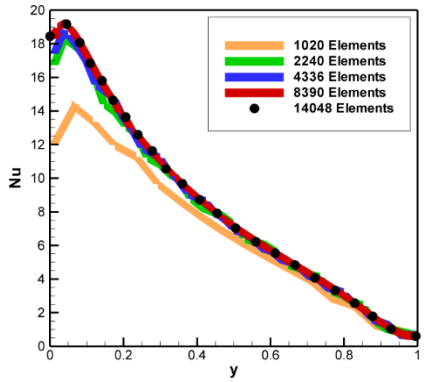

Figure 2: Local Nusselt number on the left cavity wall at $Pr = 6.2$, $Ra = 10^6$, $\phi =$ **0.02** , Ha = 25, and $\eta = 10^{-4}$

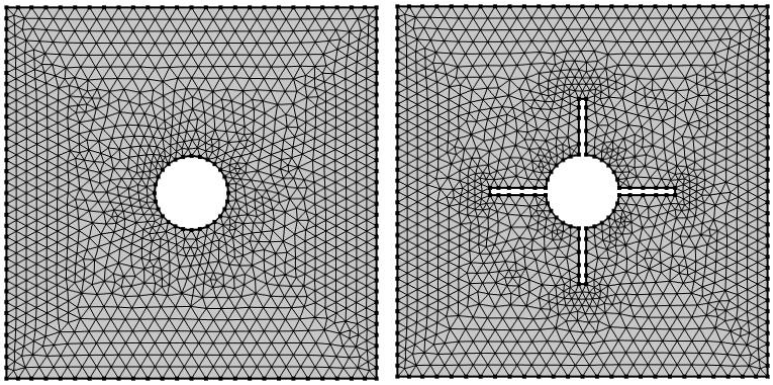

(a) (b)

Figure 3: Grid representation at same coarser level (a) no fin and (b) with fin.

4.1. Code Validation

The validated numerical scheme is compared to the findings by Dutta et al. [14] and Mahmoodi et al. [29]. The validation method verifies the correctness and reliability of the established numerical scheme by analyzing the agreement between the current results and the findings provided in the papers mentioned above. The current results are observed to closely match as in fig. 4. The scheme's validity is confirmed by the numerical results presented in Table 3. The difference between the present results and Dutta et al. [14] shows a minimal error which guarantees the accuracy of the adopted scheme.

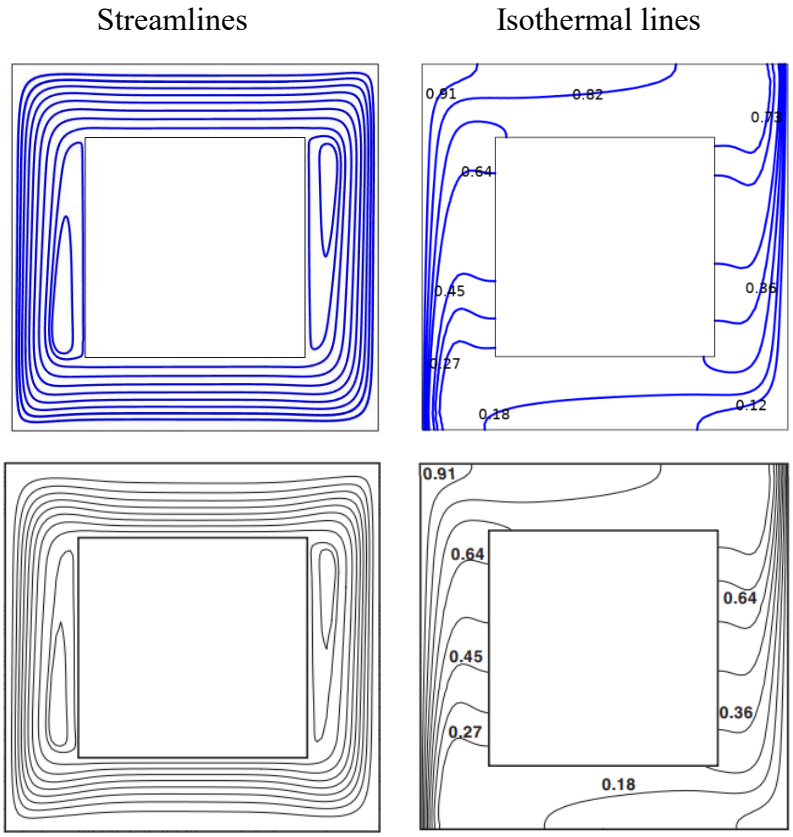

Figure 4: comparison between present results (first rom) and Mahmoodi et al. [29] (second row) for streamlines and isotherms for $Ra = 10^6$, $Pr = 6.8$ and $AR = 0.6$.

Table 3: Comparison results of averaged Nusselt number at the hot bottom wall of the cavity at $Pr = 6.2$, $Ra = 10^6$, $\phi = 0.05$ using the relation $|Ha_{new}-Ha_{[14]}|$ which compares the difference between the presents and Dutta et al. [14] in absolute terms.

Ha	Dutta et al. [14]	Present results	$\|Ha_{new} - Ha_{[14]}\|$
0	11.10	11.175	0.075
20	10.62	10.664	0.044
40	9.770	9.7053	0.065
60	8.855	8.6437	0.21
80	8.003	7.667	0.34
100	7.277	6.8369	0.44

5. Results and Discussions

In this section, we will give a detail description of two-dimensional natural convection flow in a square cavity with four fins and a circular cylinder inside it. The major study encircles the effect of fin length, fin position in terms of rotational angle, Hartmann number, Prandtl number, Nano particles volume fraction and Rayleigh number. The flow parameters will be investigated in the range as, $0^0 \leq \alpha \leq 75^0$ with step size of 15^0, l is varied from 0 to 0.5 with increment of 0.02, Ra lies in the range $10^2 \leq Ra \leq 10^8$, $Pr = (0.7, 6.2, 25)$, $0 \leq Ha \leq 100$ and $0 \leq \phi \leq$. The fluid is considered as a homogenous mixture of copper nano particles and incompressible. Simulation is performed to examine flow pattern, heat convection and irreversibility in proposed problem. The computed results are shown in the form of figures and tables.

Figure 5 shows the rotational angle between $0^0 \leq \alpha \leq 75^0$ on streamlines and isotherms, results indicates that when the rotating angle is increased, the streamlines become more curved, resulting to more shift in the flow direction. Reduced rotational angle, on the other hand, results in fewer curved streamlines and a smoother shift in the flow direction. Higher rotational angles produce stronger vortices, resulting in tighter and more concentrated circular flow patterns. Vortices may be weaker or less pronounced at lower rotational angles. Flow separation happens when a flow detaches from a surface or an item, resulting in recirculated zones. Higher rotational angles encourage flow separation and the creation of recirculation zones along streamlines.

Similarly for isotherms as indicated in Fig. 5, Higher rotating angles facilitate heat redistribution and mixing, resulting in a more homogenous temperature distribution along the isotherms. Lower rotational angles may limit mixing and cause localized temperature fluctuations. By increasing the rotating angle, the thickness of the thermal boundary layers is reduced, resulting in quicker heat transfer and more rapid temperature fluctuations along the isotherms. Increasing the rotational angle of a fins on the heat exchanger can result in a more equal distribution of temperature along isotherms. Reducing the rotational angle, on the other hand, may result in temperature gradients and unequal heat transmission. Table 4 shows the average Nusselt numbers and entropy when the fin rotates from $\alpha = 0^0$ and $\alpha = 75^0$. The Nusselt number increases with rotation up to 60^0 and decreases with rotation to 75^0. A similar phenomenon exists for entropy owing to heat and magnetism, and a continuous increment was seen for entropy due to viscous friction.

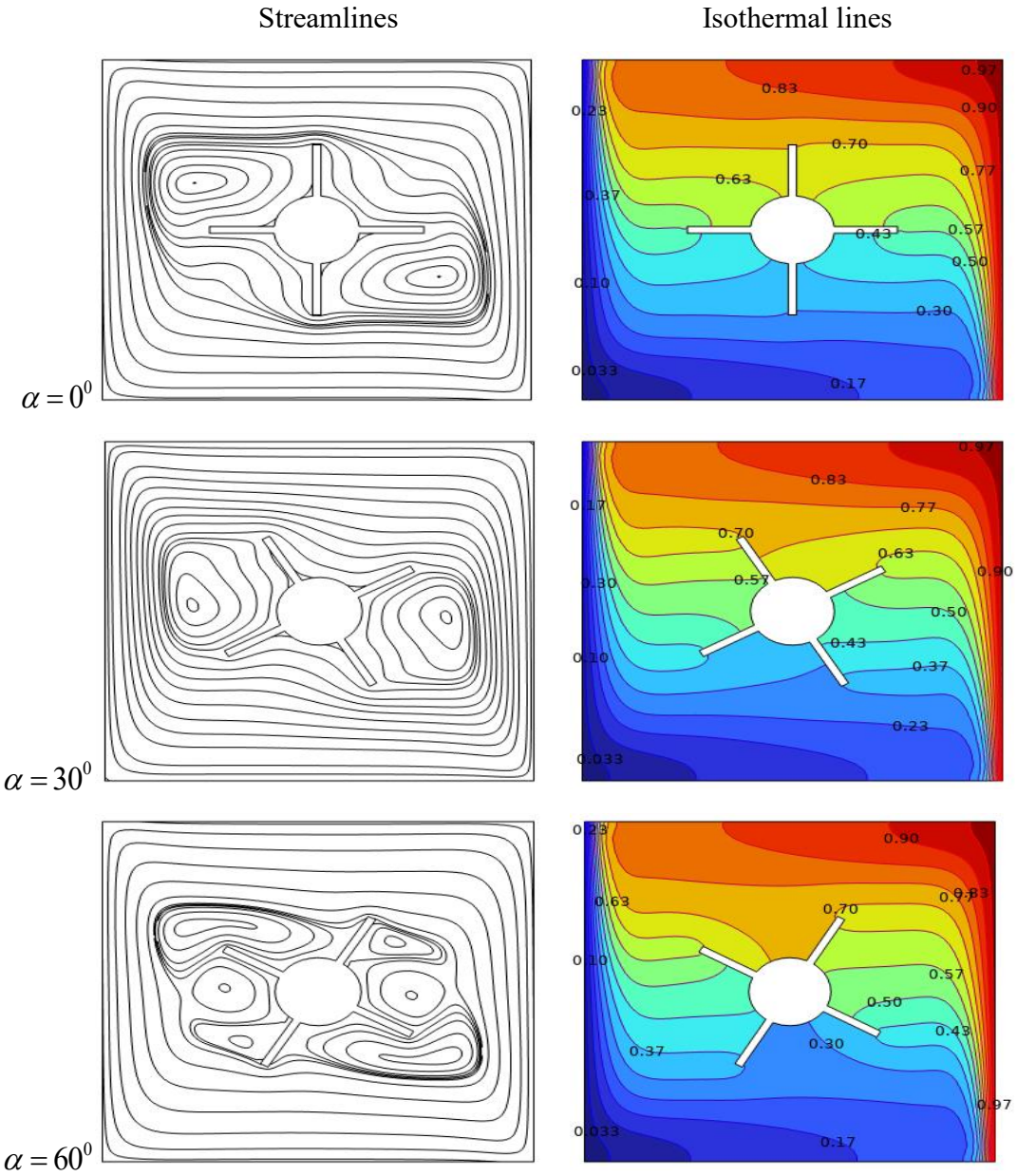

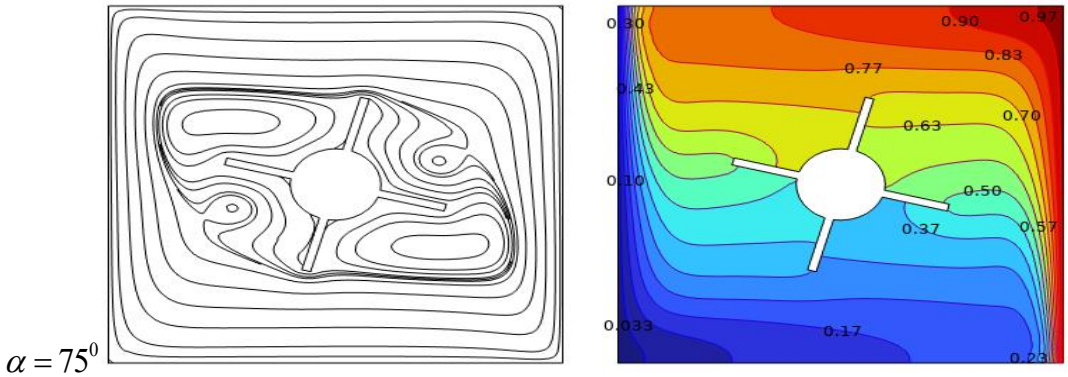

$\alpha = 75^0$

Figure 5: Effects of rotational angle (a) $\alpha = 0^0$, (b) $\alpha = 30^0$, (c) $\alpha = 60^0$ (d) $\alpha = 75^0$ on streamlines and isotherms for Pr = 6.2, Ra = 10^6, $\phi = 0.02$, Ha = 25, and $\eta = 10^{-4}$

Table 4: The Nu_{avg}, $\overline{S}_h$, $\overline{S}_f$ and $\overline{S}_m$ values for various α using Pr = 6.2, Ra = 10^6, ϕ= 0.02, Ha = 25, and η = 10^{-4}

α	Nu_{avg}	$\overline{S}_h$	$\overline{S}_f$	$\overline{S}_m$
0^0	8.3057	8.6512	231.5	141.15
15^0	8.3071	8.6503	230.75	141.8
30^0	8.3166	8.6594	229.38	142.43
45^0	8.3293	8.6761	228.55	142.14
60^0	8.3332	8.6781	229.92	141
75^0	8.3191	8.6642	231.24	140.73

For streamlines in general, a longer fin has a higher surface area for heat transmission. This is presented in Fig. 6 which shows the effects of fin length on streamlines and isotherms, the rows indicate no fin, l = 15w and l = 25w respectively. Because of the larger surface area, more fluid particles encounter the fin, resulting in improved convective heat transmission. As a result, the streamlines tend to bend more around the fin, resulting in a bigger boundary layer and increased flow resistance. Similarly, a shorter fin, on the other hand, has a reduced surface area for heat transmission. As a result, convective heat transmission is decreased, and the boundary layer is smaller. As a result, streamlines travel through the fin with less deviation, resulting in decreased flow resistance.

For isotherms, a longer fin will cause a greater surface area available for heat transmission with a longer fin. This results in better heat dissipation and a more equal temperature distribution over the length of the fin. As a result, isotherms are more regularly distributed and parallel to the surface of the fin, indicating a more efficient cooling process. Similarly, the accessible surface area for heat transmission reduces when the fin length is lowered. This can result in greater temperatures near the fin's base, closer to the heat source, and less uniform temperature distribution over the length of the fin. As a result, the isotherms may become more distorted and deviate from their parallel arrangement, suggesting decreased cooling effectiveness. While larger fins typically provide better heat dissipation due to higher surface area, there is a practical limit to fin length. Excessively long fins might cause additional problems such as greater pressure drop, higher production costs, or structural limits. As a result, optimizing fin length entails a variety of criteria and trade-offs based on the unique application and needs. Table 5 shows the impacts of altering fin length on Average Nusselt and entropy generation, and it is possible to see that when fin length varies from $0 \leq l \leq 0.5$, both average Nusselt number and entropy rise, although at a slow rate. This is because the surface area accessible for heat transmission increases as the fin length increases. This increased surface area can lead to improved convective heat transmission. As a result, as fin length increases, so does the average Nusselt number. Increasing the length of the fin may cause more flow disturbances and interactions between the fin and the surrounding fluid. These modifications can enhance the system's complexity and disorder, potentially leading to higher entropy creation.

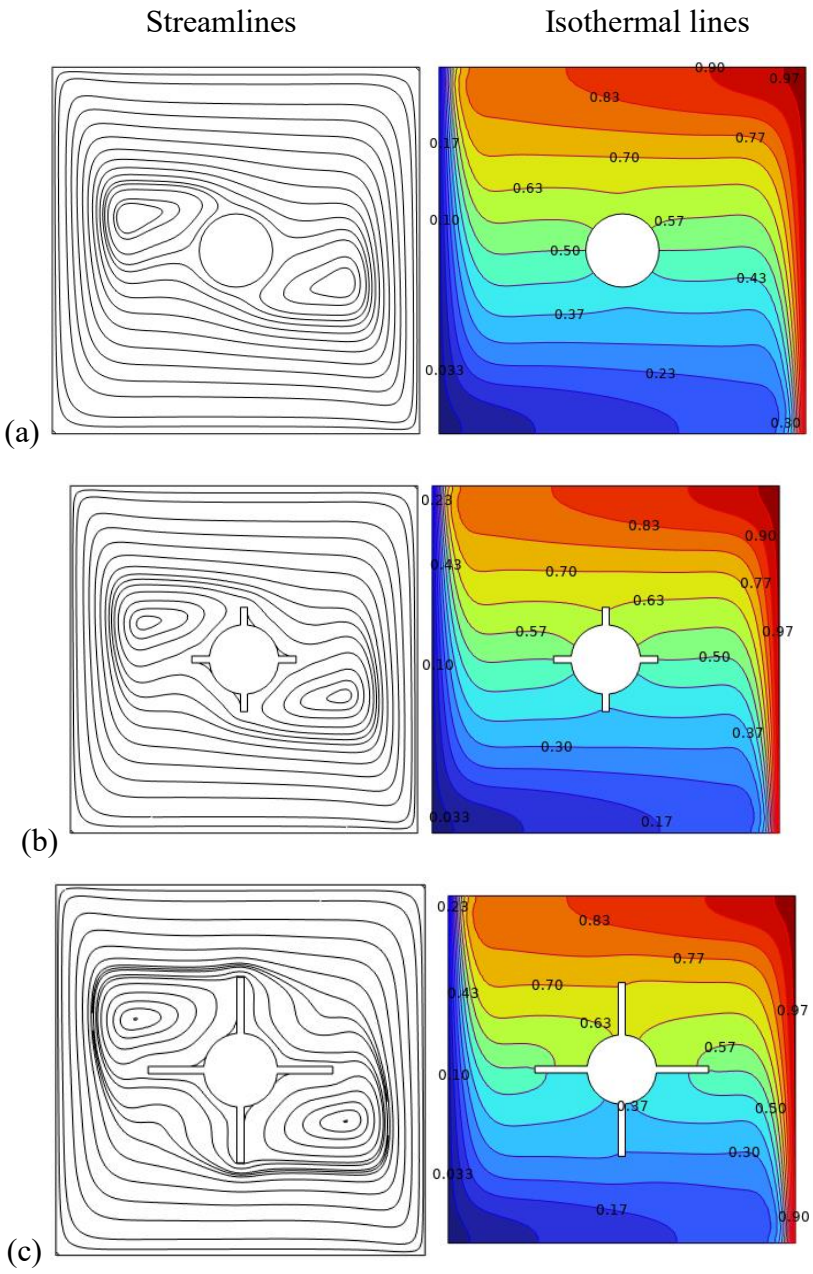

Figure 6: Effects of fin length on streamlines and isotherms, (a) first row no fin (b) second row $l = 15w$ and (c) last row $l = 25w$ for Pr = 6.2, $Ra = 10^6$, $\phi = 0.02$, $\alpha = 0^0$, $Ha = 25$, and $\eta = 10^{-4}$

Table 5: The Nu_{avg}, $\overline{S}_h$, $\overline{S}_f$ and $\overline{S}_m$ values by varying the fin length for Pr = 6.2, Ra = 10^6, ϕ= 0.02, α = 0^0, Ha = 25, and η = 10^{-4}

	Nu_{avg}	$\overline{S}_h$	$\overline{S}_f$	$\overline{S}_m$
No fin	8.2633	8.4986	226.06	142.41
l = 0.22	8.2646	8.5079	226.31	142.49
l = 0.24	8.2653	8.5159	226.45	142.53
l = 0.26	8.2649	8.5252	226.69	142.55
l = 0.28	8.2682	8.5341	226.96	142.58
l = 0.3	8.2696	8.5445	227.2	142.55
l = 0.32	8.2758	8.5539	227.46	142.55
l = 0.34	8.2776	8.5645	227.75	142.49
l = 0.36	8.2802	8.5755	228.07	142.42
l = 0.38	8.2838	8.5871	228.37	142.31
l = 0.4	8.2878	8.5969	228.77	142.21
l = 0.42	8.2924	8.6074	229.2	142.08
l = 0.44	8.2944	8.6192	229.69	141.88
l = 0.46	8.2999	8.6297	230.21	141.67
l = 0.48	8.3016	8.6406	230.8	141.42
l = 0.5	8.3057	8.6512	231.5	141.15

Figure 7 shows flow pattern might vary as Ra rises and the effects of *Ra* on streamlines and isotherms, *Ra* = 10^2, 10^6, 10^8. Lower Ra values may result in a primarily laminar flow with smooth and well-defined streamlines. Higher Ra levels frequently result in higher flow velocities and better mixing. With higher intermingling of fluid packages, the streamlines may display more complicated patterns, facilitating better mixing of heat or mass within the flow. The creation of vortices becomes more noticeable with higher Ra levels. Vortices may cause swirling motion and fluid packages to follow complicated trajectories, resulting in more complex streamlines with loops and eddies.

Figure 7 further shows that for isotherms of *Ra* influences the temperature distribution inside a fluid. The temperature differences between the fins and the surrounding fluid grow increasingly apparent as *Ra* rises. The slopes of the isotherms tend to be steeper, suggesting greater temperature variations over the flow field. Ra influences the thickness of thermal boundary layers around the fins. Because of enhanced convective heat transmission, higher Ra values result in thinner boundary layers, which later result in quicker heat transfer rates and faster temperature shifts along isotherms. Ra can be increased to facilitate heat dissipation from the fins. The isotherms around the fins spread out further, indicating improved heat transmission and a greater region of effect. This aids in heat dissipation and sustaining lower temperatures in the system. Table 6 shows how the Rayleigh number affects the average Nusselt number, and entropy due to heat, viscosity, and magnetism. As Ra varies, there has been a general rise in Nusselt number and entropy, this is because higher Ra numbers imply stronger buoyancy-driven flows, resulting in improved convective heat transfer which forces the Nusselt number to increase. Entropy tends to rise when heat transfer is in place, and the system evolves toward a more disordered state.

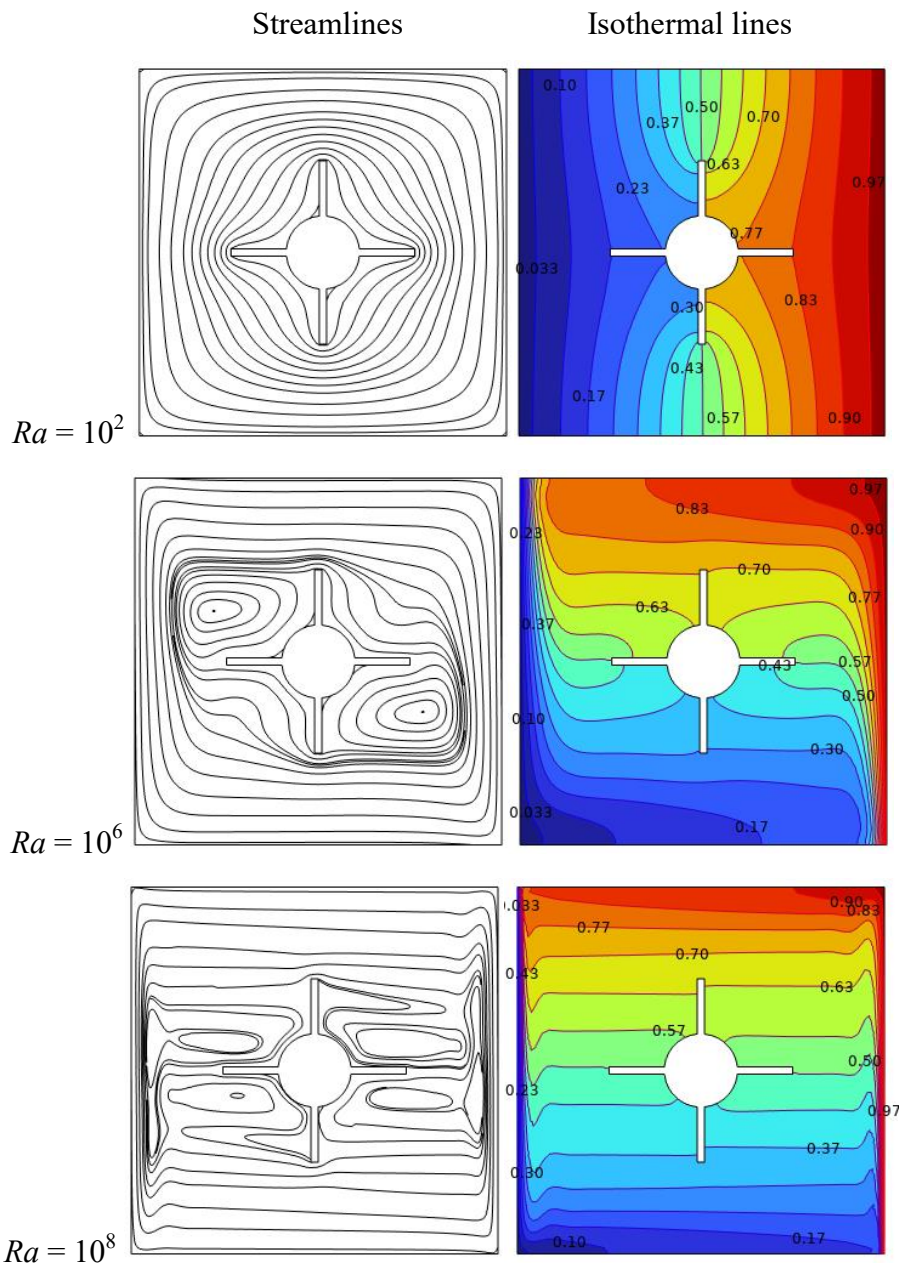

Figure 7: Effects of Ra on streamlines and isotherms, (a) $Ra = 10^2$ first row (b) $Ra = 10^6$ second row and (c) $Ra = 10^8$ last row for Pr = 6.2, l=25w, ϕ = 0.02, $\alpha = 0^0$, Ha = 25, and $\eta = 10^{-4}$

Table 6: Effects of *Ra* on Nu_{avg}, $\overline{S}_h$, $\overline{S}_f$ and $\overline{S}_m$ for Pr = 6.2, *l*=25*w*, ϕ= 0.02, α = 0^0, Ha = 25, and η = 10^{-4}

Ra	Nu_{avg}	$\overline{S}_h$	$\overline{S}_f$	$\overline{S}_m$
10	0.8477	0.88604	2.16E-07	4.25E-07
10^2	0.84776	0.88609	2.16E-05	4.25E-05
10^3	0.85247	0.89094	0.002152	0.004238
10^4	1.1752	1.2274	0.18836	0.35419
10^5	3.5024	3.6541	7.7608	10.278
10^6	8.3057	8.6512	231.5	141.15
10^7	16.882	17.621	5549.4	1273
10^8	30.661	32.704	1.06E+05	8818.8

The magnetohydrodynamic effect, also known as the Hartmann effect, is the influence of a magnetic field on the flow of an electrically conducting fluid. The Hartmann effect can influence several parameters in heat transmission, including the average Nusselt number and entropy production. Table 7 shows the effect of Hartmann on the fluid flow. At Ha=0 the effect on entropy due to magnet is also negligeable. However, as Ha starts to increase both average Nusselt number and entropy at all levels tends to reduce. This is because Ha effect can affect the convective heat transfer properties, causing the Nusselt number to vary. The flow behavior of the conducting fluid can be changed in the presence of a magnetic field, resulting in changing heat transfer rates and, as a result, influencing the Nusselt number. The irreversible development of entropy caused by temperature changes inside a system is referred to as entropy generation owing to heat transfer. When there is a temperature differential in a fluid, heat transmission happens, and entropy is produced. The presence of a magnetic field can change temperature distribution and heat transmission properties, hence impacting heat-induced entropy production. The Hartmann effect can inhibit fluid velocity in some instances, modifying the temperature profile and diminishing temperature gradients. This decrease in temperature gradients has the potential to reduce entropy formation owing to heat transfer. The Hartmann effect has the potential to modify fluid flow properties such as velocity profiles and pressure distributions, hence influencing entropy formation owing to fluid friction. Fluid mobility can be changed in the presence of a magnetic field, resulting in changes in flow patterns and pressure losses. As a result, the Hartmann effect can alter the entropy production caused by fluid friction. The magnitude of this alteration is determined by elements such as magnetic field intensity, fluid characteristics, and geometrical configuration. This entropy creation is caused by the magnet's loss of magnetic energy into heat because of the fluid's electrical conductivity. As a result of the interaction between the magnetic field and the conducting fluid, the Hartmann effect can alter the entropy production caused by the magnet. The presence of a magnetic field affects fluid dynamics and produces extra dissipative processes that contribute to the generation of entropy.

Dissipation influences convective heat transport inside a system, which in turn influences the average Nusselt number. Table 8 presence the dissipation effect with respect to average Nusselt number and entropy due to heat, friction, and magnet. As dissipation increase from 0 to 0.1 the average Nusselt number and entropy due to heat are on the increase, while entropy due to fiction and magnet decreases rapidly. This is because energy losses in fluid flow are increased by dissipative processes such as viscous friction. These losses lower the convective heat transfer coefficient (h) and change the temperature distribution, influencing the average Nusselt number (Nu). Higher degrees of dissipation, in general, tend to increase convective heat transfer and hence the average Nusselt number. Dissipation adds to the creation of entropy in a system owing to heat transmission. Temperature gradients are formed as mechanical energy is turned into thermal energy, resulting in heat transfer and entropy creation. Heat-induced dissipation-related entropy formation happens via a variety of methods, including viscous dissipation and thermal conduction. As more mechanical energy is transformed into thermal energy, the temperature gradients and heat transport within the system are amplified. Because of fluid friction, these energy losses appear as heat, resulting in increased entropy generation. Higher degrees of dissipation amplify energy losses, resulting in higher entropy formation due to fluid friction. The creation of dissipation-related entropy in this scenario results from the conversion of magnetic energy into thermal energy inside the fluid. Magnetic energy is wasted, and entropy is formed while the conducting fluid undergoes resistive heating. Higher degrees of dissipation, such as enhanced electrical conductivity or stronger magnetic fields, might intensify the dissipation-related entropy production associated with the magnetic field-fluid interaction.

The Prandtl number affects convective heat transmission by altering the thickness of the boundary layer and temperature gradients. Larger Prandtl numbers suggest a larger ratio of momentum diffusivity to thermal diffusivity, implying that heat is more easily transferred than fluid motion. Table 9 presents the effects of Prandtl on average Nusselt number and entropy due to heat, friction, and magnet. As Prandtl number changes from gas to water to argon, the effect on average Nusselt number, entropy due to heat, friction, and magnet all tends to increase. This is because smaller thermal boundary layer and faster heat transfer rates, which increases the average Nusselt number. The Prandtl number influences entropy formation due to heat transport as well. Heat transfer happens when temperature gradients exist in a fluid, resulting in entropy formation. The Prandtl number impacts the temperature distribution and consequently the development of entropy due to heat. Greater Prandtl number imply greater thermal diffusivity in comparison to momentum diffusivity. Heat is transmitted more effectively than fluid motion, resulting in lower temperature gradients and decreased entropy formation owing to heat transmission. fluid friction leads to the development of entropy. The Prandtl number influences flow properties such as velocity profiles and pressure distributions, which in turn impact entropy formation owing to fluid friction. Higher Prandtl values imply higher viscosity in comparison to thermal diffusivity, which results in increased fluid friction. This results in increased entropy formation owing to fluid friction. The Prandtl number can also influence the creation of entropy owing to the interaction of a magnetic field and a conducting fluid. The development of entropy results from the dissipation of magnetic energy into heat because of the fluid's electrical conductivity. The Prandtl number affects flow and thermal properties, which in turn affect dissipation and entropy production. Higher Prandtl numbers can result in more heat conduction relative to fluid velocity, which can result in increased entropy creation owing to the magnet.

Table 7: Effects of *Ha* on Nu_{avg}, $\overline{S}_h$, $\overline{S}_f$ and $\overline{S}_m$ for Pr = 6.2, *l*=25*w*, ϕ= 0.02, $\alpha = 0^0$, Ha = 25, and $\eta = 10^{-4}$

Ha	Nu_{avg}	$\overline{S}_h$	$\overline{S}_f$	$\overline{S}_m$
0	9.5004	9.8922	392.85	0
10	9.2714	9.6545	353.02	36.803
20	8.6796	9.0397	271.71	108.39
30	7.9086	8.2383	195.49	168.21
40	7.1059	7.4036	138.21	204.3
50	6.3543	6.6216	98.349	220.77
60	5.6866	5.9266	71.234	224.32
70	5.1078	5.324	52.762	220.23
80	4.6104	4.8061	40.015	212.01
90	4.1833	4.3612	31.058	201.79
100	3.8153	3.9777	24.637	190.81

Table 8: Effects of ϕ on Nu_{avg}, $\overline{S}_h$, $\overline{S}_f$ and $\overline{S}_m$ for Pr = 6.2, $l=0$, $\alpha = 0^0$, Ha = 25, and $\eta = 10^{-4}$

ϕ	Nu_{avg}	$\overline{S}_h$	$\overline{S}_f$	$\overline{S}_m$
0	8.2353	8.5771	239.26	147.28
0.01	8.2712	8.6148	235.28	144.15
0.02	8.3057	8.6512	231.5	141.15
0.03	8.3389	8.6862	227.92	138.28
0.04	8.3709	8.7199	224.52	135.52
0.05	8.4017	8.7524	221.29	132.87
0.06	8.4315	8.7839	218.22	130.32
0.07	8.4603	8.8143	215.31	127.87
0.08	8.4882	8.8439	212.54	125.5
0.09	8.5153	8.8725	209.92	123.22
0.1	8.5415	8.9003	207.43	121.01

Table 9: Effects of *Pr* on Nu_{avg}, $\overline{S}_h$, $\overline{S}_f$ and $\overline{S}_m$ for $l=0$, $\alpha = 0^0$, Ha = 25, and $\eta = 10^{-4}$

Pr	Nu_{avg}	$\overline{S}_h$	$\overline{S}_f$	$\overline{S}_m$
0.7	8.1077	8.45	220.55	125.51
6.2	8.3057	8.6512	231.5	141.15
25	8.3152	8.6604	232.45	142.51

6. Conclusion

The findings of the study have important practical implications for the design and optimization of heat transfer systems. The research advances our understanding of the fundamental principles that drive heat transport and entropy generation for obstacles with fins, allowing for greater thermal efficiency and energy conservation in a variety of engineering applications. The application of various Hartmann numbers, Rayleigh numbers, and particle volume fractions adds to our understanding of flow behavior and temperature distribution in relation to fin characteristics, paving the way for more efficient and sustainable thermal management solutions. From the findings the following results were discovered: Higher rotational angles encourage flow separation and the creation of recirculation zones along streamlines. Increasing the length of the fin causes more flow disturbances and interactions between the fin and the surrounding fluid that results to higher heat transfer and entropy generation. Higher Ra values result in thinner boundary layers, which result in quicker heat transfer rates and faster temperature shifts along isotherms. The presence of a magnetic field affects fluid dynamics and produces extra dissipative processes that contribute to the generation of entropy. Higher degrees of dissipation, such as enhanced electrical conductivity or stronger magnetic fields, might intensify the dissipation-related entropy production associated with the magnetic field-fluid interaction. Higher Prandtl numbers can result in more heat conduction relative to fluid velocity, which can result in increased entropy generation owing to the magnet.

Data availability statement: Data will be available on request.

Conflict of Interest statement: All authors have confirmed that they have no economic or private affiliations that might be seen as influencing the work disclosed in this publication.

References

1. Hosseini, M. J., Rahimi, M., & Bahrampoury, R. (2015). Thermal analysis of PCM containing heat exchanger enhanced with normal annular fines. Mechanical Sciences, 6(2), 221-234.
2. Dindarloo, M. R., & Payan, S. (2019). Effect of fin thickness, grooves depth, and fin attachment angle to the hot wall on

maximum heat transfer reduction in a square enclosure. International Journal of Thermal Sciences, 136, 473-490.
3. Tayebi, T., Dogonchi, A. S., Karimi, N., Ge-JiLe, H., Chamkha, A. J., & Elmasry, Y. (2021). Thermo-economic and entropy generation analyses of magnetic natural convective flow in a nanofluid-filled annular enclosure fitted with fins. Sustainable Energy Technologies and Assessments, 46, 101274.
4. Ye, W., & Khodadadi, J. M. (2022). Effects of arrow-shape fins on the melting performance of a horizontal shell-and-tube latent heat thermal energy storage unit. Journal of Energy Storage, 54, 105201.
5. Lemouedda, A., Breuer, M., Franz, E., Botsch, T., & Delgado, A. (2010). Optimization of the angle of attack of delta-winglet vortex generators in a plate-fin-and-tube heat exchanger. International journal of heat and mass transfer, 53(23-24), 5386-5399.
6. Yu, C., Xue, X., Shi, K., Wang, R., Zhang, L., & Shao, M. (2021). Optimization of wavy fin-and-elliptical tube heat exchanger using CFD, multi-objective genetic algorithm and radical basis function. Energy Science & Engineering, 9(9), 1359-1372.
7. Muhammad, T., Alsaedi, A., Hayat, T., & Shehzad, S. A. (2017). A revised model for Darcy-Forchheimer three-dimensional flow of nanofluid subject to convective boundary condition. Results in physics, 7, 2791-2797.
8. Ganesh, N. V., Hakeem, A. A., & Ganga, B. (2018). Darcy–Forchheimer flow of hydromagnetic nanofluid over a stretching/shrinking sheet in a thermally stratified porous medium with second order slip, viscous and Ohmic dissipations effects. Ain Shams Engineering Journal, 9(4), 939-951.
9. Hossain, M. A., Saleem, M., & Gorla, R. S. R. (2013). Surface-radiation effect on natural convection flow in a fluid-saturated non-Darcy porous medium enclosed by non-isothermal walls. International Journal of Numerical Methods for Heat & Fluid Flow, 23(8), 1320-1339.
10. Abu-Nada, E., Masoud, Z., Oztop, H. F., & Campo, A. (2010). Effect of nanofluid variable properties on natural convection in enclosures. International Journal of Thermal Sciences, 49(3), 479-491.
11. Khanafer, K., Vafai, K., & Lightstone, M. (2003). Buoyancy-driven heat transfer enhancement in a two-dimensional enclosure utilizing nanofluids. International journal of heat and mass transfer, 46(19), 3639-3653.
12. Kuwahata, A., Kusakabe, M., Chikaki, S., Saito, I., & Sekino, M. (2020). Cavity-shaped magnet for highly sensitive magnetic detection of magnetic nanoparticles in breast cancer patients. AIP Advances, 10(1).
13. Geridonmez, B. P., & Oztop, H. F. (2019). Natural convection in a cavity filled with porous medium under the effect of a partial magnetic field. International Journal of Mechanical Sciences, 161, 105077.
14. Dutta, S., Pati, S., & Baranyi, L. (2021). Numerical analysis of magnetohydrodynamic natural convection in a nanofluid filled quadrantal enclosure. Case Studies in Thermal Engineering, 28, 101507.
15. Dulikravich, G. S., & Lynn, S. R. (1997). Unified electro-magneto-fluid dynamics (EMFD): Introductory concepts. International Journal of Non-Linear Mechanics, 32(5), 913-922.
16. Eringen, A. C., & Maugin, G. A. (2012). Electrodynamics of continua I: foundations and solid media. Springer Science & Business Media.
17. Bourantas, G. C., Skouras, E. D., Loukopoulos, V. C., & Nikiforidis, G. C. (2009). An accurate, stable and efficient domain-type meshless method for the solution of MHD flow problems. Journal of Computational Physics, 228(21), 8135-8160.
18. Pirmohammadi, M., & Ghassemi, M. (2009). Effect of magnetic field on convection heat transfer inside a tilted square enclosure. International Communications in Heat and Mass Transfer, 36(7), 776-780.
19. Pirmohammadi, M., Ghassemi, M., & Sheikhzadeh, G. A. (2008, June). The effect of a magnetic field on buoyancy-driven convection in differentially heated square cavity. In 2008 14th Symposium on Electromagnetic Launch Technology (pp. 1-6). IEEE.
20. Alchaar, S., Vasseur, P., & Bilgen, E. (1995). The effect of a magnetic field on natural convection in a shallow cavity heated from below. Chemical Engineering Communications, 134(1), 195-209.
21. Al-Najem, N. M., Khanafer, K. M., & El-Refaee, M. M. (1998). Numerical study of laminar natural convection in tilted enclosure with transverse magnetic field. International Journal of Numerical Methods for Heat & Fluid Flow, 8(6), 651-672.
22. Baytaş, A. C. (2000). Entropy generation for natural convection in an inclined porous cavity. International Journal of Heat and Mass Transfer, 43(12), 2089-2099.
23. BaytaŞ, A. C., & BaytaŞ, A. F. (2005). Entropy generation in porous media. In Transport Phenomena in Porous Media III (pp. 201-226). Pergamon.
24. Shah, Z., Ullah, A., Musa, A., Vrinceanu, N., Ferrandiz Bou, S., Iqbal, S., & Deebani, W. (2022). Entropy optimization and thermal behavior of a porous system with considering hybrid nanofluid. Frontiers in Physics, 10, 929463.
25. Saleem, M., Hossain, M. A., Mahmud, S., & Pop, I. (2011). Entropy generation in Marangoni convection flow of heated fluid in an open ended cavity. International Journal of Heat and Mass Transfer, 54(21-22), 4473-4484.
26. Alzahrani, A. K., Sivasankaran, S., & Bhuvaneswari, M. (2020). Numerical simulation on convection and thermal radiation of Casson fluid in an enclosure with entropy generation. Entropy, 22(2), 229.
27. Stampolidis, P., & Gousidou-Koutita, M. C. (2018). A computational study with finite difference methods for second order quasilinear hyperbolic partial differential equations in two independent variables. Applied Mathematics, 9(11), 1193-1224.
28. Ho, C. J., Chen, M. W., & Li, Z. W. (2008). Numerical

simulation of natural convection of nanofluid in a square enclosure: effects due to uncertainties of viscosity and thermal conductivity. International Journal of Heat and Mass Transfer, 51(17-18), 4506-4516.
29. Mahmoodi, M., & Sebdani, S. M. (2012). Natural convection in a square cavity containing a nanofluid and an adiabatic square block at the center. Superlattices and Microstructures, 52(2), 261-275.
30. Abbas, S. Z., Wang, X., Khan, W. A., Hobiny, A., & Iqbal, K. (2022). Finite element analysis of nanofluid flow and heat transfer in a square cavity with two circular obstacles at different positions in the presence of magnetic field. Journal of Energy Storage, 51, 104462.
31. Charreh, D., Islam, S. U., & Saleem, M. (2023). Entropy Generation Analysis on Natural Convection in a Non-Darcy Porous Square Cavity with Thermal Radiation and Viscous Dissipation. Available at SSRN 4446307.
32. Kim, J., Kang, Y. T., & Choi, C. K. (2004). Analysis of convective instability and heat transfer characteristics of nanofluids. Physics of fluids, 16(7), 2395-2401.
33. Abdel-Nour, Z., Aissa, A., Mebarek-Oudina, F., Rashad, A. M., Ali, H. M., Sahnoun, M., & El Ganaoui, M. (2020). Magnetohydrodynamic natural convection of hybrid nanofluid in a porous enclosure: numerical analysis of the entropy generation. Journal of Thermal Analysis and Calorimetry, 141, 1981-1992.